OPTICA

Reconfigurable photon localization by coherent drive and dissipation in photonic lattices

O. Jamadi,[1,†,5] B. Real,[1,†] K. Sawicki,[2] C. Hainaut,[1] A. González-Tudela,[3] N. Pernet,[4] I. Sagnes,[4] M. Morassi,[4] A. Lemaître,[4] L. Le Gratiet,[4] A. Harouri,[4] S. Ravets,[4] J. Bloch,[4] and A. Amo[1,*]

[1]Univ. de Lille, CNRS, UMR 8523–PhLAM–Physique des Lasers, Atomes et Molécules, Lille, France
[2]Institute of Experimental Physics, Faculty of Physics, University of Warsaw, Pasteura St. 5, 02-093 Warsaw, Poland
[3]Institute of Fundamental Physics IFF-CSIC, Calle Serrano 113b, 28006 Madrid, Spain
[4]Université Paris-Saclay, CNRS, Centre de Nanosciences et de Nanotechnologies, 91120, Palaiseau, France
[5]e-mail: omar.jamadi@gmail.com
*Corresponding author: alberto.amo-garcia@univ-lille.fr

Received 3 January 2022; revised 19 April 2022; accepted 28 April 2022; published 27 June 2022

The engineering of localized modes in photonic structures is one of the main targets of modern photonics. An efficient strategy to design these modes is to use the interplay of constructive and destructive interference in periodic photonic lattices. This mechanism is at the origin of the defect modes in photonic bandgaps, bound states in the continuum, and compact localized states in flat bands. Here, we show that in lattices of lossy resonators, the addition of external optical drives with a controlled phase enlarges the possibilities of manipulating interference effects and allows for the design of novel types of localized modes. Using a honeycomb lattice of coupled micropillars resonantly driven with several laser spots at energies within its photonic bands, we demonstrate the localization of light in at-will geometries down to a single site. These localized modes are fully reconfigurable and have the potentiality of enhancing nonlinear effects and of controlling light–matter interactions with single site resolution.

https://doi.org/10.1364/OPTICA.452624

1. INTRODUCTION

Engineering the localization of light in dielectric structures is one of the main targets of modern micro- and nano-photonics. From a fundamental point of view, the study of localization in photonic materials has allowed understanding the subtle interplay of disorder, periodicity, and quasi-crystalline order [1–3]. Localized modes are useful for enhancing light–matter interactions, increasing the non-linear response of a material, and storing information in a reduced volume. A very successful strategy for engineering localized modes in optics is to use lattices of coupled waveguides, coupled resonators, or photonic crystals. In these periodic structures, localized modes at predefined wavelengths and spatial locations can be engineered by carefully designing the bulk eigenmodes or by introducing defects in the bandgaps. Examples of the first type are the modes localized by disorder (Anderson localization) in a lattice [1,2], the compact localized states of a flat band [4–6], the bound states in the continuum (BIC) [7–10], and localized modes in lattices with gain and loss close to the parity-time symmetric condition [11]. To the second type belong the localized modes in the gap separating two photonic bands when a local potential is added to the otherwise periodic structure. This is actually the principle of photonic crystal cavities and of Tamm modes at the surface of a photonic system [12–14]. Recently, the use of bands with non-trivial topology has allowed the implementation of localized modes at the edges and corners of photonic lattices of different dimensionalities without the need of introducing local on-site potentials [15–22]. The edge or corner modes appear because of the topology of the bulk, with the important asset being that their existence and optical frequency are protected from certain types of disorder.

One of the main limitations to the above-mentioned designs is that the underlying interference mechanism responsible for localization presents fundamental limits for the localization length, which is generally larger than a single lattice site. For instance, compact localized states in flat bands arise from the interference between at least two lattice sites with non-zero amplitude and opposite phases [23,24]. Similarly, bound states in the continuum involve light intensity in several sites [10,25] and localization by disorder requires multiple scatterers. In all cases, the localized modes are eigenmodes of the system, whose amplitude distribution is independent of the external excitation conditions. Another important limitation is that the modes are localized by design, that is, the geometry of the dielectric structure sets the location, shape, and extension of the localized modes. This implies that after fabrication these properties are hardly adjustable.

In this paper, we demonstrate a method to engineer fully reconfigurable localized modes in photonic lattices of coupled resonators, with localization lengths covering several sites as small

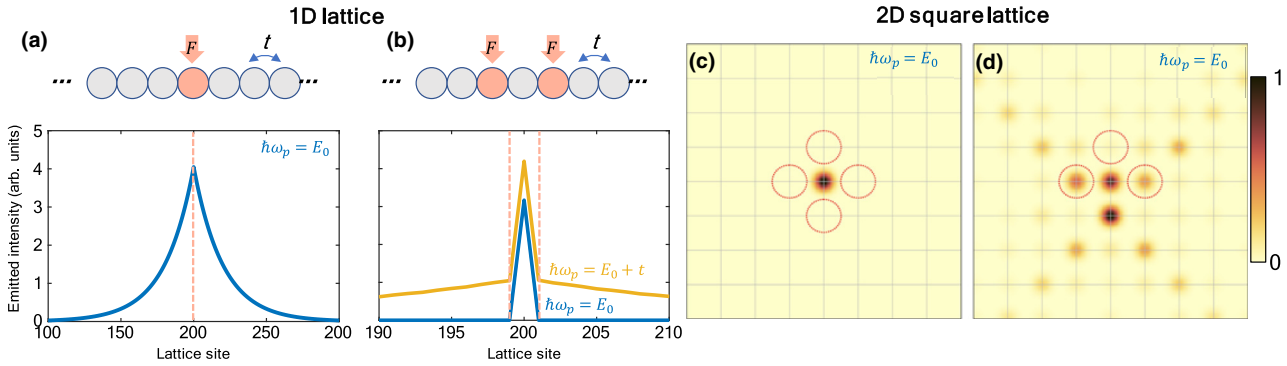

Fig. 1. Localized modes in a driven-dissipative lattice. (a) A one-dimensional lattice with 400 sites resonantly driven by a laser located at a single site at the energy of the middle of the photonic band, showing propagation of the emitted intensity with a decay length of $\sim t\tau/\hbar$ sites, with $\tau = 10\hbar/t$. (b) When two drives of the same amplitude and phase envelope a single site, the emission is fully localized in the middle site (blue line). Away from the resonance frequency $\hbar\omega_p = \varepsilon_0$, emission extends over the whole lattice (orange line). The vertical lines mark the position of the pump lasers. (c) Calculated emission intensity in a squared lattice of 30×30 sites (zoomed view) driven at the four sites marked in red with a frequency $\hbar\omega_p = \varepsilon_0$ and identical phases. The lattice sites are located at the line crossings. (d) When one of the drive lasers is removed, emission spreads over the lattice.

as a single site. To reach this ultimate limit, we take advantage of the interplay of the coherent drive and dissipation in a lattice of lossy resonators, a mechanism that had not been previously considered for engineering localized modes. Indeed, in dissipative lattices driven at resonance, the amplitude and phase of the external driving laser provide additional knobs to engineer interference effects. By choosing the appropriate arrangement of the external drives, it is possible to implement localized modes at photon energies in which the passive system (without coherent drive) would present extended modes. Recently, the interplay of drive and losses has been used to demonstrate the trapping of light in a single site of a two coupled pillars system [26]. Here, we demonstrate that the localized response of a driven-dissipative photonic lattice can be engineered with virtually any geometry. The concept is reminiscent of wavefront shaping techniques employed to obtain a desired output through a disordered medium [27–29]. The localized modes demonstrated here in a photonic lattice can be seen as fully reconfigurable optical cavities defined by properly designing the external control field. We experimentally illustrate our method using a honeycomb lattice of coupled micropillars resonantly driven by several laser spots at energies within the photonic bands of the structure, resulting in the localization of light on a single site. Our results can be extended to a variety of mode configurations and to almost any lattice geometry in one, two, and three dimensions. They demonstrate unprecedented perspectives for the manipulation of light in photonic structures and, in particular, for enhancing local light–matter interactions and nonlinear effects with single-site precision.

2. LOCALIZATION BY DRIVE AND DISSIPATION

To demonstrate the principle of localization by drive and dissipation, we consider a lattice of coupled photonic resonators. Each of them is subject to radiative losses to the environment and can be driven by an external laser (coherent field). The archetypical system implementing this situation is a lattice of coupled semiconductor micropillars [30–33], which is the platform we use for the experimental realization. The dynamics of the photon field in a lattice of coupled micropillars in the tight-binding limit can be described by the following set of coupled equations [34]:

$$i\hbar\frac{\partial\psi_m}{\partial t} = \varepsilon_m\psi_m + \sum_n t_{m,n}\psi_n - i\frac{\hbar}{2\tau}\psi_m + F_m e^{-i\omega_p t}. \quad (1)$$

ψ_m is the field amplitude at the center of micropillar m, $\varepsilon_m = \varepsilon_0$ is the energy of the considered mode in each pillar (assumed to be identical for all sites), $t_{m,n}$ is the coupling amplitude between different sites of the lattice, τ is the radiative photon lifetime in each micropillar, and F_m is the complex amplitude of the resonant excitation laser at site m with photon energy $\hbar\omega_p$.

Equation (1) has a family of localized solutions for specific configurations of the drive field F_m in the steady state. Figure 1(a) shows the simplest example of a one-dimensional lattice of coupled resonators with nearest-neighbors hopping amplitude $t_{m,m+1} = t_{m,m-1} = t$ and $\tau = 10\hbar/t$. If a single site M in the middle of the lattice is pumped by a laser at any frequency within the photonic band, then the steady state intensity simulated using Eq. (1) extends over many lattice sites (on the order of $t\tau/\hbar$ for the particular case of $\hbar\omega_p = \varepsilon_0$). Remarkably, in the configuration of Fig. 1(b), in which two sites $M-1$ and $M+1$ are pumped with equal phase and amplitude at $\hbar\omega_p = \varepsilon_0$, the response of the lattice is almost fully localized at site M, which is surrounded by the two pumps. The field intensity in the pumped sites is almost zero, as well as in all lattice sites located out of the region defined by the two pumps (it tends strictly to zero for long lifetimes, when $\hbar/\tau \ll t_{m,n}$). This behavior is reminiscent of the Fabry–Perot bound states in the continuum based on coupled resonances [8,10,25].

This kind of localized mode is a general feature of Eq. (1). When a region of the one-dimensional lattice is delimited by two pump spots of the same absolute amplitude $|F|$, it can be shown that in the limit $\tau \gg t$ there exists a discrete set of photon frequencies of the driving field for which the photon amplitude is exactly zero at the pumped sites and different from zero within the region delimited by the pumps (see Supplement 1). Because the pumped sites have zero amplitude, the pump frequency at which this phenomenon takes place coincides precisely with the eigenenergies of the region confined by the pumps as if it was fully detached from the lattice. In the case of Fig. 1(b), this is the eigenenergy of a single site decoupled from the rest of the lattice ($\hbar\omega_p = \varepsilon_0$). Simultaneously, the zero-field amplitude in the pumped sites results, strictly, in zero amplitude of the photon field outside the confined region

(see Supplement 1 for an analytic proof). This means that the presence of the localized mode is independent of the lattice size out of the confined region. Note that if the frequency of the drive is shifted from the resonant condition, then the emitted intensity is distributed over all lattice sites, as demonstrated by the slow decay of the emission out of the central peak depicted by the orange line in Fig. 1(b).

The description we have just presented and the corresponding simulations of Eq. (1) can be directly extended to higher dimensional lattices. Figure 1(c) displays a simulation of a square lattice with four pumped sites (marked with red circles) of equal amplitude and phase surrounding a single site. An extreme localized response at $\hbar\omega_p = \varepsilon_0$, down to a single site, is observed with almost zero amplitude in the pumped sites and in the sites away from the pumped region. As a counterexample, Fig. 1(d) shows the case when the pump spots do not fully surround a central site. In this situation, the real-space distribution of the field does not show any confined response at $\hbar\omega_p = \varepsilon_0$ or at any other laser energy.

3. EXPERIMENTAL REALIZATION

Semiconductor micropillars are an ideal system for exploring the concept of localization by drive and dissipation that we have just introduced. Single micropillars can be laterally etched from planar microcavities made of two AlGaAs Bragg mirrors embedding a GaAs cavity spacer. In addition, in our structures, a single InGaAs quantum well is grown at the center of the cavity. At 6 K, the temperature of the experiments, quantum well excitons are strongly coupled to the lowest optical mode of the micropillar, giving rise to exciton-polaritons [34]. However, we work at sufficiently negative photon-exciton detuning for polaritons to have a 99% photonic content, and all the effects we report here can, in principle, be observed in structures without excitonic resonances. Each micropillar confines discrete photonic modes that can be laterally coupled in the form of a lattice by making the micropillars overlap. Here, we consider a honeycomb lattice of micropillars of 2.75 μm in diameter and a center-to-center separation of 2.3 μm [see sketch in Fig. 2(a)]. Angle-resolved photoluminescence with a non-resonant laser excitation at 1.535 eV in a 2.3 μm spot (full-width at half-maximum) centered on top of a micropillar reveals the two lowest energy bands of the structure [Fig. 2(b)]. They display two Dirac crossings characteristic of honeycomb lattices [30]. The experiments are realized in transmission geometry employing linearly polarized excitation. No significant polarization splitting is observed in the studied photonic bands. We fit the measured bands to a tight-binding model [35] with the nearest-neighbor hopping $t = 328$ μeV and the next-nearest neighbor hopping $t' = -42$ μeV. The emission energy at the Dirac crossings is $E_0 = 1.3917$ eV (see Supplement 1 for full details about samples and experimental setup). Real-space measurements of the polariton field with submicron resolution can be achieved by collecting the light emitted from the sample with a lens of 0.5 numerical aperture. The emitted light from the backside of the lattice is imaged on a CCD camera.

Under resonant laser excitation, the dynamics of the photon field in the lattice can be accurately described by Eq. (1), with the addition of a next-nearest neighbor hopping term [30]. This

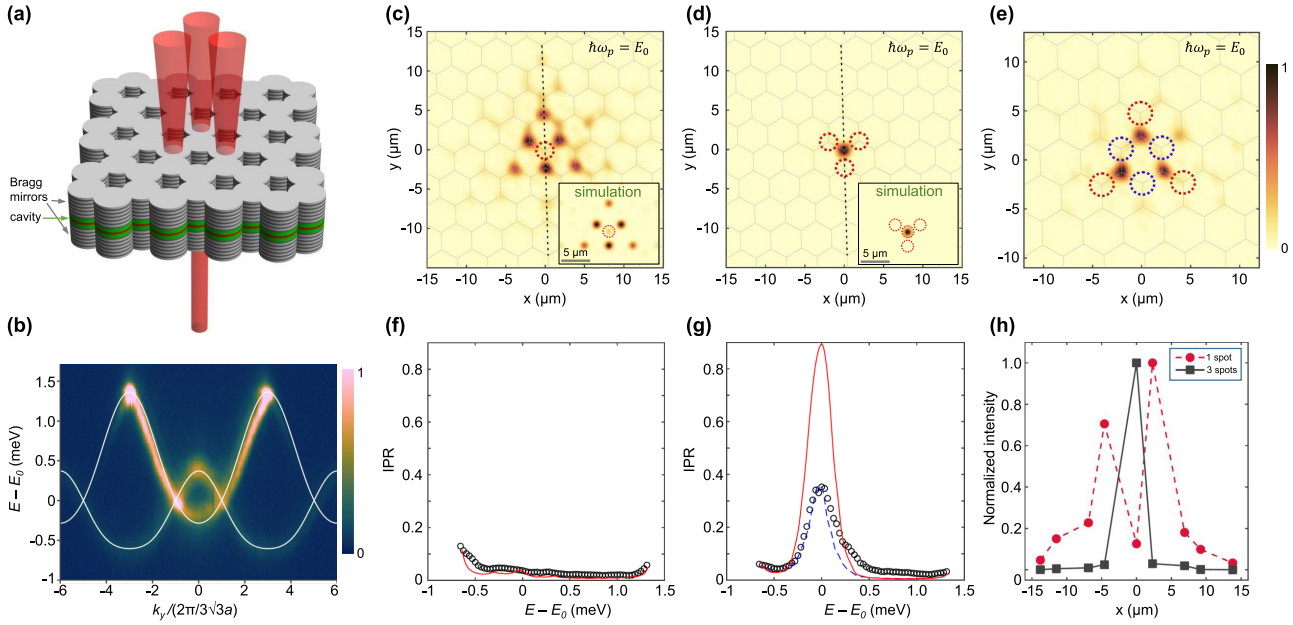

Fig. 2. Resonant drive of a honeycomb lattice. (a) The scheme of the honeycomb lattice of the micropillars and of the excitation (top) and emission (bottom) beams. (b) The measured angle-resolved photoluminescence of the lattice showing the energy bands as a function of in-plane momentum k_y for $k_x = 2\pi/3a$, with $a = 2.3$ μm the center-to-center separation between adjacent micropillars and $E_0 = 1.3917$ eV. White lines represent the tight-binding fit. (c) The measured emission pattern when driving the pillar marked with a red circle with a laser at $\hbar\omega_p = E_0$. The center of each micropillar is located at the vertices of the grey hexagonal pattern. (d) The same emission pattern when driving three pillars with equal amplitude and phase surrounding a central one, which shows high emission intensity. The insets in (c) and (d) show simulations in the conditions of the experiment. (e) The optical response when arranging three times the localization building block shown in (d) to form a staggered triangle. The laser spots in the blue sites have twice the intensity of spots in the red sites. (f) and (g) The measured IPR (dots) as a function of the laser frequency with the pump spot configurations of (c) and (d), respectively. The red lines show the calculated value using the photon lifetime of the cavity. The blue dashed line in (g) accounts for a phase difference of 0.09π between the bottom pump spot and the left one and between the right one and the bottom one. (h) The measured intensity profiles along the dashed lines in (c) and (d).

description captures the driven-dissipative nature of the micropillar system. Lattices of coupled waveguides and ring resonators are commonly described by a conservative version of Eq. (1), i.e., without pump and loss terms [16,36,37]. By adding supplementary waveguides, it is possible to resonantly drive individual sites in these systems giving access to the physics discussed here. Other experimental platforms such as lattices of mechanical resonators are well described by Eq. (1), but they have been mostly studied in a different context of nonlinear effects with drive extended to all lattice sites [38].

Figure 2(c) displays the measured intensity when pumping a single site (red circle) of the honeycomb lattice with a laser at a frequency $\hbar\omega_p = E_0$, the energy of the Dirac crossing in Fig. 2(b). The field amplitude extends away from the pump spot in a triangular shape mostly in the sites belonging to the sublattice opposite to that of the pumped micropillar. Remarkably, the pumped site shows almost no intensity. This peculiar response is a consequence of the interference effect at the pumped site between the pump laser and the eigenmodes of the lower bonding band and the upper anti-bonding band. This effect was already noticed in the simpler case of two coupled micropillars pumped at an energy right in between the bonding and anti-bonding modes [26] and also in a honeycomb lattice under strain [39]. The field distribution is very different when three laser spots of the same amplitude and phase excite the lattice in a triangular geometry surrounding a single site. This situation is reported in Fig. 2(d) using a spatial light modulator to generate the pump spots. Similar to the simulations for the square lattice shown in Fig. 1(c), the field distribution is strongly localized in the micropillar surrounded by the three pump spots, and no significant emission anywhere else in the lattice is observed (including the pumped sites) [see Fig. 2(h)]. The measured real-space patterns are well reproduced by numerically solving Eq. (1) in the steady-state regime [see insets of Figs. 2(c) and 2(d)]. The simulations include the next-nearest-neighbors hopping with the value extracted from the fits to the polariton bands and a polariton lifetime of $\tau = 9$ ps.

The extreme localized response, down to a single micropillar, can be quantified by computing the inverse participation ratio (IPR), $\mathrm{IPR} = \sum_m |\psi_m|^4 / \sum_m |\psi_m|^2$, which has a value of 1 for emission fully localized in a single site and 0 for extended modes in an infinite lattice. Figure 2(g) depicts the measured IPR for the three laser spots excitation as a function of the laser photon energy from the bottom to the top of the Dirac bands. The IPR is computed from the emission measured at the center of each micropillar. The transmitted pattern is highly localized at the energy of the Dirac point (E_0, IPR = 0.35). This photon energy is very close to the estimated eigenenergy ε_0 of the fundamental mode of a single detached micropillar ($E_0 = \varepsilon_0 + 3t'$), and they would both coincide exactly in the absence of next-nearest-neighbor coupling. Simulations of Eq. (1) are displayed in red lines and predict a value of IPR = 0.89 for the measured polariton lifetime. The difference with the measured value of 0.35 arises from an unintentional horizontal tilt of the incident laser beams, which induces an estimated phase difference of about 0.09π between the three consecutive spots. In the limit of negligible losses, simulations show that the IPR grows asymptotically towards 0.9 (it would be one in the absence of the next-nearest-neighbors hopping, see Supplement 1). Moreover, localization is highly preserved in the presence of a mild disorder (see Supplement 1). In contrast, Fig. 2(f) shows that for a single spot excitation, the transmitted signal is extended over several lattice sites for any photon energy resulting in very low IPR values.

The localized mode with three pumping spots shown in Fig. 2(d) can now be used as a building block to engineer any possible intensity pattern in the lattice, just by adding groups of three laser spots of the same phase at the energy of the Dirac points. An example is shown in Fig. 2(e) with a staggered triangle of three emitting sites. To engineer it, we have used three groups of three excitation spots each. Each group surrounds one of the emitting pillars. The overall excitation spot distribution is highlighted in the figure by dashed circles, the blue ones having twice as much intensity as the red ones.

So far, we have discussed single-site localized modes, which appear close to the energy of an isolated micropillar. We now address drive-induced localization in multiple adjacent sites. In this case, the localization resonances appear at the molecular eigenenergies of the considered ensemble of sites encircled by the coherent drives. To explore this situation, we move to a configuration of pump spots of equal amplitude and phase surrounding completely two adjacent pillars of the honeycomb lattice, as sketched in red circles in Fig. 3(b). In that configuration, we would expect a localized mode at the energy of the bonding states of two coupled isolated sites $\hbar\omega_p = E_0 - t$. Figure 3(a) displays the measured IPR as a function of the laser energy from the bottom to the top of the photonic bands. A peak of localization appears at $\hbar\omega_p = E_0 - 0.36$ meV, which is very close to the expected value (the difference arising from the presence of the next-nearest-neighbor hopping). Spatial localization in a pattern very close to that of the bonding-like mode is shown in Fig. 3(b). For comparison, Fig. 3(c) displays the measured spatial pattern at $\hbar\omega_p = E_0$, showing a significant spread. The origin of the low value of the measured IPR peak is that the four drive spots do not have the exact same phase due to a slight misalignment in the experimental setup. Under perfect alignment conditions, the calculated IPR peak has a value 0.32, about four times higher than in the experiment [see Fig. 3(d)]. Localization at the energy of the anti-bonding two-sites mode of the confined molecule is observed at $\hbar\omega_p \approx E_0 + t$ when the upper two pump spots have a phase difference of π with respect to the two lower pump spots (see Supplement 1).

As demonstrated above, the photon energy at which the localized mode takes place is determined by the eigenenergies of the optically confined cavities as if they were detached from the lattice. We will now show that the resonance energy for high localization can be modified at will, at least in the simplest cases, by adding an additional pump spot on top of the localized sites. We consider again the situation with three identical pump spots depicted in Fig. 2(d), which results in localization at a single site. On top of this localized site, we add an additional drive of the same frequency as the surrounding laser spots. Remarkably, the resonance frequency for the localization is now modified, as shown in the simulations in Fig. 4(a). The magnitude of the frequency shift is determined by the relative amplitude of the added spot F_{in} compared to that of the surrounding spots F_{out}. The sign of the shift, towards higher or lower energies, is set by its phase, 0 or π with respect to the phase of the surrounding pump spots. For the photon lifetime of our experiments, the IPR of the localized mode has some variations with frequency related to the shape of the photon dispersion and the density of states of the lattice. Figure 4(b) shows that these variations are smoothed for long photon lifetimes.

Figure 4(c) displays the measured IPR as a function of the laser frequency when the intensity of the additional central spot is three

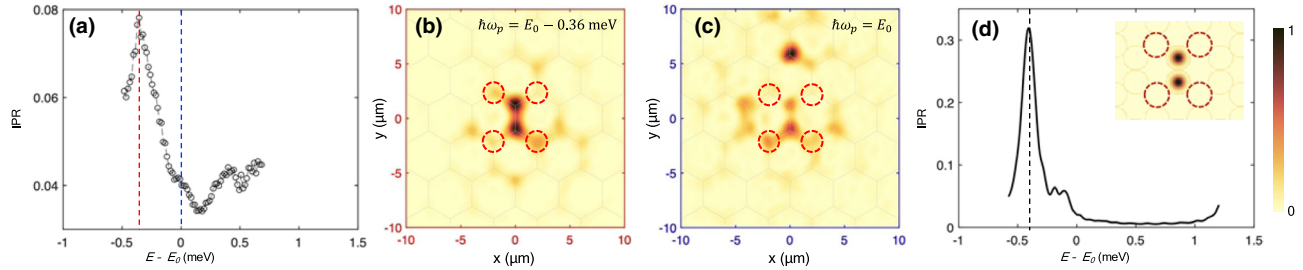

Fig. 3. Localized bonding mode. (a) The measured IPR when four driving spots of nominally the same amplitude and phase demarcate a two-site molecule. For photon energies above $E_0 + 0.7$ meV, residual scattered light prevents a confident measurement of the IPR. (b) The measured emitted intensity at the IPR peak [red dashed line in (a)]: $\hbar\omega_p = E_0 - 0.36$ meV. The pump spots are drawn in red circles. (c) The measured emission intensity at $\hbar\omega_p = E_0$ [blue dashed line in (a)]. (d) The simulated IPR in the case of perfect optical alignment. The inset shows the simulated intensity distribution at $\hbar\omega_p = E_0 - 0.407$ meV (corresponding to the dashed line in the main panel).

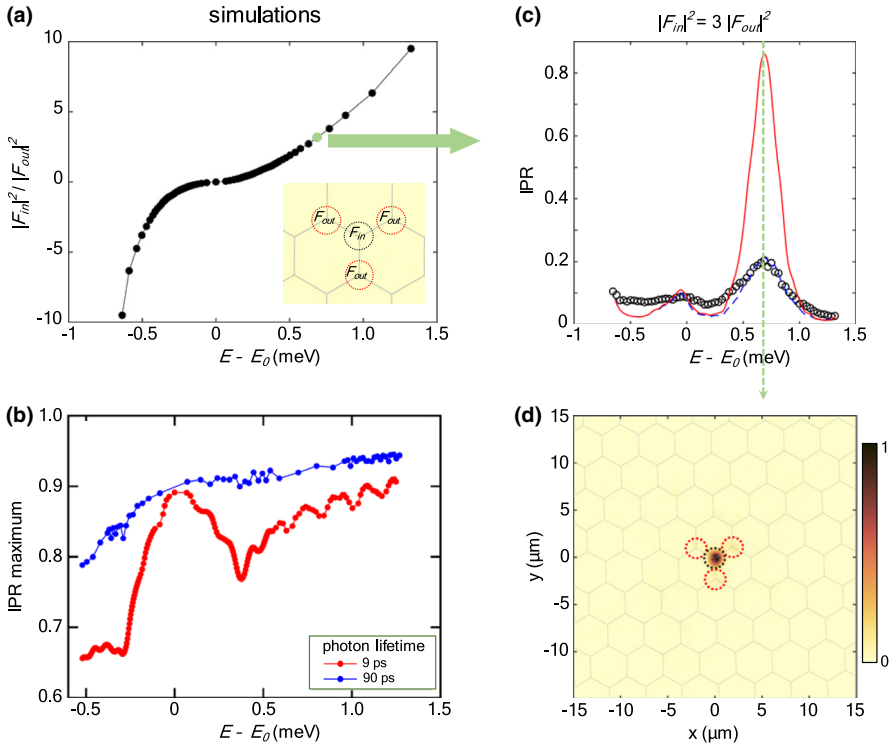

Fig. 4. Modifying the energy of the localized mode. (a) The calculated photon energy of the IPR peak for the four spots configuration shown in the inset. The vertical axis shows the ratio of intensities of the central pump spot $|F_{\text{in}}|^2$ to the outer three spots $|F_{\text{out}}|^2$. The sign represents the relative phase between the outer and the inner spots: positive means the same phase, and negative phase means a phase difference of π. (b) The calculated value of the IPR maximum when its energy is peaked at the value indicated in the horizontal axis for two values of the photon lifetime in the resonators. (c) The measured IPR (dots) when scanning the laser frequency in the configuration of the inset in (a) for $|F_{\text{in}}|^2 = 3 \times |F_{\text{out}}|^2$ [green dot in (a)]. The red line is the calculated IPR using the photon lifetime of the lattice and equal phase for the four spots. The blue line includes a phase difference of 0.05π for one of the outer spots. (d) The real-space emission measured at the energy of the IPR peak ($E - E_0 = 0.69$ meV).

times larger than that of the surrounding spots and, nominally, the same phase. The IPR peak is shifted from E_0 to $E_0 + 0.69$ meV. Figure 4(d) shows a highly localized emission at a single site at that photon energy.

4. DISCUSSION

We have demonstrated that the combination of the resonant drive and dissipation in the lattices of the coupled photonic resonators can be advantageously used to design highly localized emission patterns in a reconfigurable manner with high flexibility. Alternatively, to the comprehensive design scheme we have presented here, reverse engineering can be directly employed by solving Eq. (1) in the steady regime for the excitation fields F_m after imposing a desired shape and frequency of the photon field in the lattice. These features can be directly transposed to other photonic systems, such as lattices of superconducting microwave cavities [40], resonators with spectral synthetic dimensions [41,42], (opto)mechanical lattices [43] and, more generally, to fluid wave systems [44]. They could be used to locally enhance nonlinear effects, for instance, in polariton lattices with high exciton content and for the control of light–matter interactions that require single-site excitation in a dense matrix. This is the case when the resonator cavity contains

single photon emitters whose emission properties may vary from site to site [45].

Interestingly, the kind of localized modes observed here are analogous to the localized emission patterns expected from quantum emitters in photonic lattices discussed in Refs. [46–49]. In our realization, the role of the quantum emitter coupled to the lattice is played by the resonant pump spots. Beyond localized modes, those theoretical works have shown the possibility of engineering highly directional responses in the lattice and that the decay dynamics can be strongly modified by the photonic density of states. These promising ideas could be directly transposed to the configuration discussed in our work in a purely photonic realization [50] and enlarge the possibilities of manipulating light–matter interactions in lattices of resonators.

Funding. Ministerio de Ciencia, Innovación y Universidades (PGC2018-094792-B-100); Consejo Superior de Investigaciones Científicas (PTI-001); Comunidad de Madrid (CAM 2020 Y2020/TCS-6545); Narodowe Centrum Nauki (DEC-2019/32/T/ST3/00332); Agence Nationale de la Recherche (ANR-11-LABX-0007, ANR-16-CE30-0021, ANR-16-IDEX-0004 ULNE, ANR-QUAN-0003-05); European Research Council (820392, 865151, 949730), Région Hauts-de-France.

Acknowledgment. We thank Fabrice Lemoult for fruitful discussions. K.S. acknowledges the doctoral scholarship ETIUDA financed by the NCN. A.G.-T. acknowledges financial support from the Proyecto Sinérgico (NanoQuCo-CM), the CSIC Research Platform on Quantum Technologies and from Spanish project (MCIU/AEI/FEDER, EU).

Disclosures. The authors declare no conflicts of interest.

Data availability. Data underlying the results presented in this paper are not publicly available at this time but may be obtained from the authors upon reasonable request.

Supplemental document. See Supplement 1 for supporting content.

[†]These authors contributed equally to this paper.

REFERENCES

1. T. Schwartz, G. Bartal, S. Fishman, and M. Segev, "Transport and Anderson localization in disordered two-dimensional photonic lattices," Nature **446**, 52–55 (2007).
2. L. Levi, M. Rechtsman, B. Freedman, T. Schwartz, O. Manela, and M. Segev, "Disorder-enhanced transport in photonic quasicrystals," Science **332**, 1541–1544 (2011).
3. V. Goblot, A. Štrkalj, N. Pernet, J. L. Lado, C. Dorow, A. Lemaître, L. Le Gratiet, A. Harouri, I. Sagnes, S. Ravets, A. Amo, J. Bloch, and O. Zilberberg, "Emergence of criticality through a cascade of delocalization transitions in quasiperiodic chains," Nat. Phys. **16**, 832–836 (2020).
4. R. A. Vicencio, C. Cantillano, L. Morales-Inostroza, B. Real, C. Mejía-Cortés, S. Weimann, A. Szameit, and M. I. Molina, "Observation of localized states in Lieb photonic lattices," Phys. Rev. Lett. **114**, 245503 (2015).
5. S. Mukherjee, A. Spracklen, D. Choudhury, N. Goldman, P. Öhberg, E. Andersson, and R. R. Thomson, "Observation of a localized flat-band state in a photonic Lieb lattice," Phys. Rev. Lett. **114**, 245504 (2015).
6. S. Xia, A. Ramachandran, S. Xia, D. Li, X. Liu, L. Tang, Y. Hu, D. Song, J. Xu, D. Leykam, S. Flach, and Z. Chen, "Unconventional flatband line states in photonic Lieb lattices," Phys. Rev. Lett. **121**, 263902 (2018).
7. C. W. Hsu, B. Zhen, A. D. Stone, J. D. Joannopoulos, and M. Soljačić, "Bound states in the continuum," Nat. Rev. Mater. **1**, 16048 (2016).
8. G. Ordonez, K. Na, and S. Kim, "Bound states in the continuum in quantum-dot pairs," Phys. Rev. A **73**, 022113 (2006).
9. S. Longhi, "Bound states in the continuum in a single-level Fano-Anderson model," Eur. Phys. J. B **57**, 45–51 (2007).
10. Y. Plotnik, O. Peleg, F. Dreisow, M. Heinrich, S. Nolte, A. Szameit, and M. Segev, "Experimental observation of optical bound states in the continuum," Phys. Rev. Lett. **107**, 183901 (2011).
11. A. Regensburger, M.-A. Miri, C. Bersch, J. Näger, G. Onishchukov, D. N. Christodoulides, and U. Peschel, "Observation of defect states in PT-symmetric optical lattices," Phys. Rev. Lett. **110**, 223902 (2013).
12. H. Ohno, E. E. Mendez, J. A. Brum, J. M. Hong, F. Agulló-Rueda, L. L. Chang, and L. Esaki, "Observation of "Tamm states" in superlattices," Phys. Rev. Lett. **64**, 2555–2558 (1990).
13. N. Malkova, I. Hromada, X. Wang, G. Bryant, and Z. Chen, "Transition between Tamm-like and Shockley-like surface states in optically induced photonic superlattices," Phys. Rev. A **80**, 043806 (2009).
14. C. Symonds, A. Lemaître, E. Homeyer, J. C. Plenet, and J. Bellessa, "Emission of Tamm plasmon/exciton polaritons," Appl. Phys. Lett. **95**, 151114 (2009).
15. T. Ozawa, H. M. Price, A. Amo, N. Goldman, M. Hafezi, L. Lu, M. C. Rechtsman, D. Schuster, J. Simon, O. Zilberberg, and I. Carusotto, "Topological photonics," Rev. Mod. Phys. **91**, 015006 (2019).
16. M. Hafezi, S. Mittal, J. Fan, A. Migdall, and J. M. Taylor, "Imaging topological edge states in silicon photonics," Nat. Photonics **7**, 1001–1005 (2013).
17. M. C. Rechtsman, J. M. Zeuner, Y. Plotnik, Y. Lumer, D. Podolsky, F. Dreisow, S. Nolte, M. Segev, and A. Szameit, "Photonic Floquet topological insulators," Nature **496**, 196–200 (2013).
18. C. Poli, M. Bellec, U. Kuhl, F. Mortessagne, and H. Schomerus, "Selective enhancement of topologically induced interface states in a dielectric resonator chain," Nat. Commun. **6**, 6710 (2015).
19. P. St-Jean, V. Goblot, E. Galopin, A. Lemaître, T. Ozawa, L. Le Gratiet, I. Sagnes, J. Bloch, and A. Amo, "Lasing in topological edge states of a one-dimensional lattice," Nat. Photonics **11**, 651–656 (2017).
20. Y. Ota, F. Liu, R. Katsumi, K. Watanabe, K. Wakabayashi, Y. Arakawa, and S. Iwamoto, "Photonic crystal nanocavity based on a topological corner state," Optica **6**, 786–789 (2019).
21. J. Noh, W. A. Benalcazar, S. Huang, M. J. Collins, K. P. Chen, T. L. Hughes, and M. C. Rechtsman, "Topological protection of photonic mid-gap defect modes," Nat. Photonics **12**, 408–415 (2018).
22. S. Mittal, V. V. Orre, G. Zhu, M. A. Gorlach, A. Poddubny, and M. Hafezi, "Photonic quadrupole topological phases," Nat. Photonics **13**, 692–696 (2019).
23. S. Flach, D. Leykam, J. D. Bodyfelt, P. Matthies, and A. S. Desyatnikov, "Detangling flat bands into Fano lattices," Europhys. Lett. **105**, 30001 (2014).
24. L. Tang, D. Song, S. Xia, S. Xia, J. Ma, W. Yan, Y. Hu, J. Xu, D. Leykam, and Z. Chen, "Photonic flat-band lattices and unconventional light localization," Nanophotonics **9**, 1161–1176 (2020).
25. S. Weimann, Y. Xu, R. Keil, A. E. Miroshnichenko, A. Tünnermann, S. Nolte, A. A. Sukhorukov, A. Szameit, and Y. S. Kivshar, "Compact surface Fano states embedded in the continuum of waveguide arrays," Phys. Rev. Lett. **111**, 240403 (2013).
26. S. R. K. Rodriguez, A. Amo, I. Sagnes, L. Le Gratiet, E. Galopin, A. Lemaître, and J. Bloch, "Interaction-induced hopping phase in driven-dissipative coupled photonic microcavities," Nat. Commun. **7**, 11887 (2016).
27. I. M. Vellekoop and A. P. Mosk, "Focusing coherent light through opaque strongly scattering media," Opt. Lett. **32**, 2309–2311 (2007).
28. S. M. Popoff, G. Lerosey, R. Carminati, M. Fink, A. C. Boccara, and S. Gigan, "Measuring the transmission matrix in optics: an approach to the study and control of light propagation in disordered media," Phys. Rev. Lett. **104**, 100601 (2010).
29. S. Rotter and S. Gigan, "Light fields in complex media: Mesoscopic scattering meets wave control," Rev. Mod. Phys. **89**, 015005 (2017).
30. T. Jacqmin, I. Carusotto, I. Sagnes, M. Abbarchi, D. D. Solnyshkov, G. Malpuech, E. Galopin, A. Lemaître, J. Bloch, and A. Amo, "Direct observation of Dirac cones and a flatband in a honeycomb lattice for polaritons," Phys. Rev. Lett. **112**, 116402 (2014).
31. F. Baboux, L. Ge, T. Jacqmin, M. Biondi, E. Galopin, A. Lemaître, L. Le Gratiet, I. Sagnes, S. Schmidt, H. E. Türeci, A. Amo, and J. Bloch, "Bosonic condensation and disorder-induced localization in a flat band," Phys. Rev. Lett. **116**, 066402 (2016).
32. C. E. Whittaker, E. Cancellieri, P. M. Walker, D. R. Gulevich, H. Schomerus, D. Vaitiekus, B. Royall, D. M. Whittaker, E. Clarke, I. V. Iorsh, I. A. Shelykh, M. S. Skolnick, and D. N. Krizhanovskii, "Exciton polaritons in a two-dimensional Lieb lattice with spin-orbit coupling," Phys. Rev. Lett. **120**, 097401 (2018).

33. S. Klembt, T. H. Harder, O. A. Egorov, K. Winkler, H. Suchomel, J. Beierlein, M. Emmerling, C. Schneider, and S. Höfling, "Polariton condensation in *S*- and *P*-flatbands in a two-dimensional Lieb lattice," Appl. Phys. Lett. **111**, 231102 (2017).
34. I. Carusotto and C. Ciuti, "Quantum fluids of light," Rev. Mod. Phys. **85**, 299–366 (2013).
35. F. Mangussi, M. Milićević, I. Sagnes, L. Le Gratiet, A. Harouri, A. Lemaître, J. Bloch, A. Amo, and G. Usaj, "Multi-orbital tight binding model for cavity-polariton lattices," J. Phys. Condens. Matter **32**, 315402 (2020).
36. A. Szameit and S. Nolte, "Discrete optics in femtosecond-laser-written photonic structures," J. Phys. B **43**, 163001 (2010).
37. S. Afzal, T. J. Zimmerling, Y. Ren, D. Perron, and V. Van, "Realization of anomalous Floquet insulators in strongly coupled nanophotonic lattices," Phys. Rev. Lett. **124**, 253601 (2020).
38. M. Sato, B. E. Hubbard, and A. J. Sievers, "*Colloquium*: Nonlinear energy localization and its manipulation in micromechanical oscillator arrays," Rev. Mod. Phys. **78**, 137–157 (2006).
39. B. Real, O. Jamadi, M. Milićević, N. Pernet, P. St-Jean, T. Ozawa, G. Montambaux, I. Sagnes, A. Lemaître, L. Le Gratiet, A. Harouri, S. Ravets, J. Bloch, and A. Amo, "Semi-Dirac transport and anisotropic localization in polariton honeycomb lattices," Phys. Rev. Lett. **125**, 186601 (2020).
40. I. Carusotto, A. A. Houck, A. J. Kollár, P. Roushan, D. I. Schuster, and J. Simon, "Photonic materials in circuit quantum electrodynamics," Nat. Phys. **16**, 268–279 (2020).
41. K. Wang, A. Dutt, K. Y. Yang, C. C. Wojcik, J. Vučković, and S. Fan, "Generating arbitrary topological windings of a non-Hermitian band," Science **371**, 1240–1245 (2021).
42. L. Yuan, A. Dutt, and S. Fan, "Synthetic frequency dimensions in dynamically modulated ring resonators," APL Photon. **6**, 071102 (2021).
43. G. Heinrich, M. Ludwig, J. Qian, B. Kubala, and F. Marquardt, "Collective dynamics in optomechanical arrays," Phys. Rev. Lett. **107**, 043603 (2011).
44. G. Ma, M. Xiao, and C. T. Chan, "Topological phases in acoustic and mechanical systems," Nat. Rev. Phys. **1**, 281–294 (2019).
45. V. Loo, C. Arnold, O. Gazzano, A. Lemaître, I. Sagnes, O. Krebs, P. Voisin, P. Senellart, and L. Lanco, "Optical nonlinearity for few-photon pulses on a quantum dot-pillar cavity device," Phys. Rev. Lett. **109**, 166806 (2012).
46. A. González-Tudela and J. I. Cirac, "Quantum emitters in two-dimensional structured reservoirs in the nonperturbative regime," Phys. Rev. Lett. **119**, 143602 (2017).
47. A. González-Tudela and J. I. Cirac, "Exotic quantum dynamics and purely long-range coherent interactions in Dirac conelike baths," Phys. Rev. A **97**, 043831 (2018).
48. L. Leonforte, A. Carollo, and F. Ciccarello, "Vacancy-like dressed states in topological waveguide QED," Phys. Rev. Lett. **126**, 063601 (2021).
49. A. Feiguin, J. J. García-Ripoll, and A. González-Tudela, "Qubit-photon corner states in all dimensions," Phys. Rev. Res **2**, 023082 (2020).
50. A. González-Tudela, "Connecting steady-states of driven-dissipative photonic lattices with spontaneous collective emission phenomena," New J. Phys. **24**, 043001 (2022).